Chinese Chemical Letters 35 (2024) 108443

Contents lists available at ScienceDirect

Chinese Chemical Letters

journal homepage: www.elsevier.com/locate/cclet

Cocktail nano-adjuvant enhanced cancer immunotherapy based on NIR-II-triggered *in-situ* tumor vaccination

Lilin Fan[a,1], Yanwen Feng[b,1], Jiang Bian[b], Anhong Chen[b], Donglin Xie[b], Zheng Cao[a,*], Jun Yue[b,*]

[a] *Jiangsu Key Laboratory of Environmentally Friendly Polymeric Materials, School of Materials Science and Engineering, Jiangsu Collaborative Innovation Center of Photovoltaic Science and Engineering, Changzhou University, Changzhou 213164, China*
[b] *School of Biomedical Engineering, Shenzhen Campus of Sun Yat-sen University, Shenzhen 518107, China*

ARTICLE INFO

Article history:
Received 9 March 2023
Revised 9 April 2023
Accepted 11 April 2023
Available online 11 April 2023

Keywords:
Nano-adjuvant
Cocktail formulation
In-situ tumor vaccination
NIR-II photothermal effect
Anticancer immune response

ABSTRACT

Second near-infrared (NIR-II) light triggered *in-situ* tumor vaccination (ISTV) represents one of the most promising strategies in boosting the whole-body antitumor immunity. While most of previously developed nano-adjuvants for NIR-II-triggered ISTV are "all-in-one" formulations, which may indiscriminately damage both the tumor cells and the immune cells, limiting the overall effect of immune response. To overcome this obstacle, we designed a "cocktail" nano-adjuvant by physically mixing hyaluronidases (HAase)-decorated gold nanostars (HA) for NIR-II light triggered *in situ* production of tumor-associated antigens and CpG functionalized gold nanospheres (CA) for immune cells activation. Compared to "all-in-one" formulation, the "cocktail" nano-adjuvants displayed a significantly stronger immune response on NIR-II light induced dendritic cells (DCs) mutation and T cells differentiation, greater effect on tumor-growth inhibition, and higher efficacy in inhibition of pulmonary metastases. What is more, increasing the molar ratio of HA to CA led to an enhanced anticancer immune responses. This study highlight the nano-adjuvant formulation effects on the treatment of tumors with multiple targets.

With the development of advanced nanotechnology, various immunotherapy strategies have emerged as a paradigm shift towards the malignant tumor treatments [1–11]. Particularly for *in-situ* tumor vaccination (ISTV), one of the most promising approaches in pursuit of personalized cancer immunotherapy, has received considerable interests due to its ease of producing a broad-spectrum of epitopes and capability in triggering whole-body anticancer immune response [12–18]. In general, ISTV involves two essential processes: one is the *in-situ* production of tumor-associated antigens (TAAs) within tumors by specific local tumor irradiations; while the other involves the activation of immune cells by adjuvants to generate anticancer immune responses, *e.g.* activation of antigen presenting cells to capture, process, and present antigens to T cells, and proliferation of antigen-stimulated T cells or recruitment of natural killer cells to induce adaptive immunity. Among approaches of local tumor irradiation, photothermal ablation of tumor cells using light in the second near-infrared II (NIR-II) window displayed superb advantages with regard to bio-safety, noninvasiveness and deep-tissue penetration [19–22].

Recently, we developed a robust nano-adjuvant platform (CHA) based on NIR-II-adsorbable gold nanostars (AuNS) whose surface were decorated with hyaluronidases (HAase) and CpG oligodeoxynucleotides for deep tumor penetration and immune activation, respectively [19]. Although successful ISTV has been achieved, this "all-in-one" nano-adjuvant formulation has an intrinsic problem: because CHA could be taken up by both the tumor cells and immune cells with a high-efficiency due to the presence of CpG ligands [23,24], the heat generated by NIR-II light irradiation could not only induce the apoptosis of cancer cells but also cause serious damage to immune cells, leading to the decrease of available immune cells within tumors. Therefore, how to minimize the heat damage to immune cells, while at the same time keeping the high-efficacy of photothermal ablation of tumor cells is still a challenge.

To overcome the above obstacles, here we designed a "cocktail" nano-adjuvant formulation composed of two spatially separated components: CpG functionalized gold nanospheres (CA, Fig. 1a) and HAase-decorated AuNS (HA, Fig. 1b), where the former was used to activate the immune cells, while the latter acted to

* Corresponding authors.
E-mail addresses: zcao@cczu.edu.cn (Z. Cao), yuejun3@mail.sysu.edu.cn (J. Yue).
[1] These authors contributed equally to this work.

https://doi.org/10.1016/j.cclet.2023.108443
1001-8417/

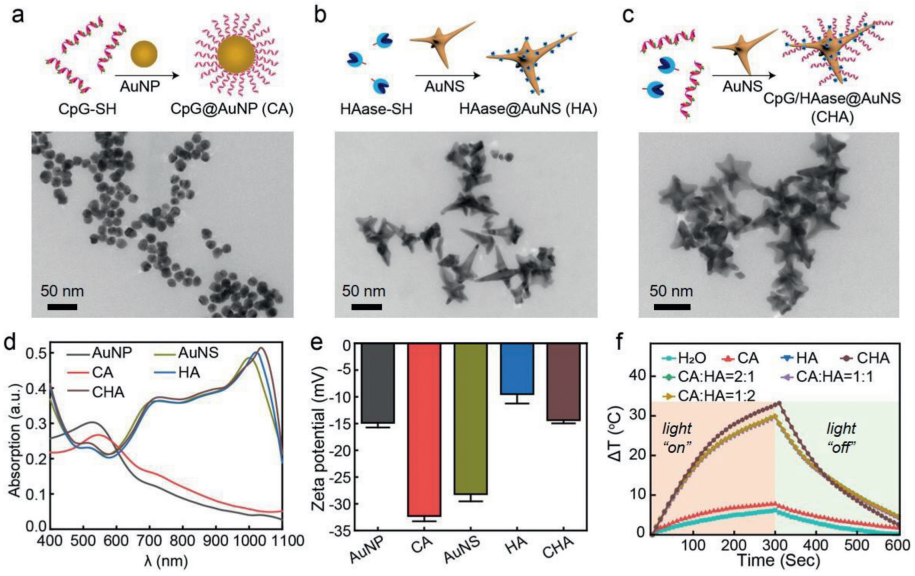

Fig. 1. Synthesis and characterizations of different formulations of gold nano-adjuvants (NAs). (a-c) Schematic illustrations and TEM images of CpG-conjugated gold nanospheres (a), HAase-conjugated gold nanostars (b), and CpG/HAase-co-functionalized gold nanostars (c). (d, e) Ultraviolet-visible (UV–vis) spectra (d) and surface charge analysis (e) of gold nanoparticles with different surface functionalizations. (f) Photothermal evaluations of NAs under 1064 nm light irradiation (1.0 W/cm^2).

Table 1
Quantitative analysis of the surface composition and photothermal conversion efficiency.

Nano-adjuvants (NAs) formulations		# CpG[a]	# HAase[b]	PCE_{NIR-II}[c]
CpG carried by AuNP (CA)		532 ± 78	N/A	12.21%
HAase carried by AuNS (HA)		N/A	1183 ± 62	34.04%
CpG and HAase co-functionalized AuNS (CHA)		718 ± 53	1146 ± 59	38.55%
Cocktail NAs	CA:HA=2:1	N/A	N/A	32.72%
	CA:HA=1:1	N/A	N/A	33.44%
	CA:HA=1:2	N/A	N/A	33.83%

[a] The average number of CpG per nanoparticle.
[b] The average number of HAase per nanoparticle.
[c] Photothermal conversion efficiency (PCE) of NAs.
N/A: not applicable.

generate TAAs upon NIR-II irradiation. Anisotropic AuNS have been identified as one of the most promising gold nanocarriers due to their superior photothermal conversion efficiency in the second near-infrared range, excellent biocompatibility and ease of surface functionalization. The conjugation of HAase on the surface of AuNS enables the deep tumor penetration. The transfer of CpG from original AuNS surface to a spherical nanoparticle surface had two advantages. On the one hand, the uptake of HA by immune cells might be largely decreased because of the absence of CpG, and CAs taken by immune cells would not absorb NIR-II light because their surface plasmon resonance peaks locate at the visible wavelength range, both of which could minimize the NIR-II light induced heat damage to immune cells; On the other hand, the "cocktail" formulation provides a feasibility in screening rational ratio between photothermo-contributing constitute (HA) and the immunostimulation-contributing constitute (CA) in pursuit of an optimal antitumor immunity. Systematic *in vivo* immune response analysis and tumor-inhibition investigations were performed to give a comprehensive understanding whether the "cocktail" nano-adjuvant was better than "all-in-one" formulation. All animal experiments were carried out according to the instruction of Animal Care and Use Committee of Sun Yat-sen University (SYSU-IACUC-2019-B718).

In this study, the cocktail formulation of nano-adjuvant (cNA) was prepared by physically mixing HA and CA under a specific ratio. As a comparison, an "all-in-one" formulation with CpG and HAase co-loaded on a single AuNS (CHA) was prepared as well (Fig. 1c). Transmission electron microscope (TEM) images showed that spherical CA had an average diameter of 25 nm (Fig. 1a), while HA and CHA displayed a multi-branched structure bearing 2–4 short tips and 1–2 long tips with an overall tip-to-tip distance around 50–80 nm (Figs. 1b and c). After loading CpG or HAase to AuNP or AuNS, the localized surface plasmon resonance (LSPR) peaks of these gold nanoparticles all had a 26–45 nm red-shift, and the LSPR peak of CA located at the visible region (556 nm), while that of HA (1042 nm) and CHA (1061 nm) were at the near-infrared region (Fig. 1d). The surface charge of gold nanoparticles changed from −28 mV to −9 mV for HAase-conjugation, and from −15 mV to −32 mV for CpG functionalization (Fig. 1e). Moreover, the conjugation process did not affect the activity of HAase toward the degradation of hyaluronic acid (Fig. S1 in Supporting information). All these data indicated the successful loading of CpG or/and HAase on each specific gold nanoparticles. Quantitative information was shown in Table 1.

Next, to investigate whether the presence of spherical CA in cocktail NAs influences the NIR-II photothermal effect of gold nanostars, each NA solution was illuminated with a 1640 nm light and the temperature changes (ΔT) were recorded as a function of time. As shown in Fig. 1f, comparing with CA, who only showed a slight temperature increase under the NIR-II light irradiation, the overall ΔT of HA, CHA and all cocktail NAs with different CA/HA ratios (but under a same concentration of HA) could rapidly increase to 30 °C over 5 min and there was no significant difference among different cocktail NA solutions, indicating that the mixing

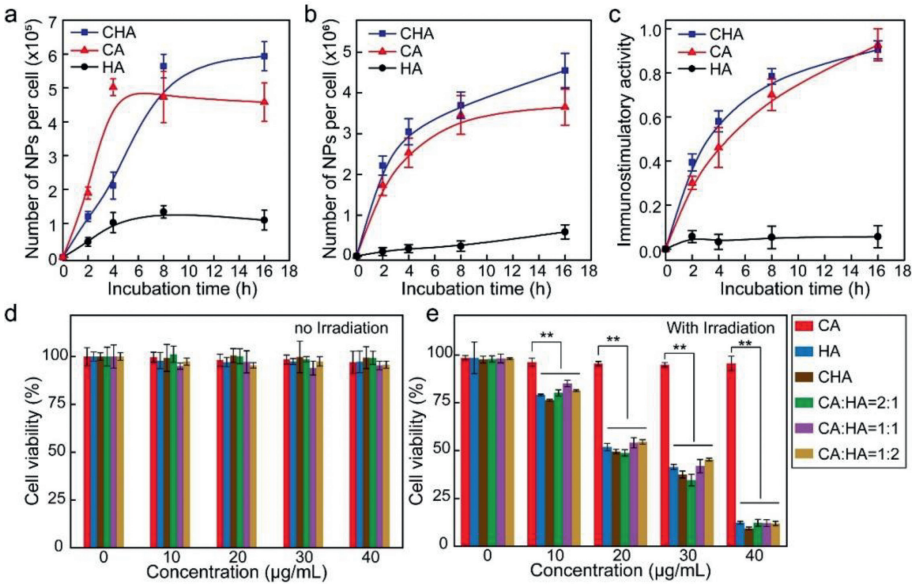

Fig. 2. Cellular uptake and NIR-II light induced cytotoxicity of different formulations of NAs. (a, b) Cellular uptake kinetics of CA, HA and CHA with 4T1 breast cancer cell line (a) or RAW 264.7 macrophages (b). (c) Immunostimulatory activity of CA, HA and CHA towards RAW-Blue cells by measuring the secreted embryonic alkaline phosphatase levels in cell media *via* the colorimetric enzyme assay based on the QUANTI-Blue reagent. (d, e) Cytotoxicity of different formulations of NAs in absence (d) or presence (e) of 1064-nm light irradiation (1.0 W/cm^2 for 5 min). Data were expressed as means ± standard error of the mean (S.E.M.) ($n = 3$) with the significant differences determined by the unpaired *t*-test, $^{**}P < 0.01$.

of CA with HA did not influence the NIR-II photothermal effect of HA. Moreover, all nanostar-containing groups displayed a high photothermal stability in five successive heating-cooling cycles under 1064 nm irradiation (Fig. S2 in Supporting information).

To figure out whether different formulations of NAs have different cellular uptake profiles, we determined the cell uptake kinetics of CA, HA and CHA by the inductively coupled plasma mass spectrometry (ICP-MS). The breast cancer cell line 4T1 and the typical immune cell line RAW 264.7 macrophages were chosen for investigations respectively. As shown in Figs. 2a and b, two CpG-containing NAs (CA and CHA) exhibited a much higher cell uptake efficacy than only-HAase-containing NAs (HA) at all examined time points for both cell lines, which could be ascribed to the interactions between oligonucleotides (rather than enzymes) on NP surface and cell membrane that accelerated the particle endocytosis *via* the scavenger-receptor-mediated mechanism. Compared to CHA who may unavoidably damage the immune cells upon NIR-II light irradiation due to their high intracellular distribution, the extreme low-efficacy of HA in entering immune cells, on the other hand however, provides an advantage in minimizing the NIR-II-induced thermal damage to immune cells.

Subsequently, we determined the immunostimulatory (IS) activity of CpG-containing NAs in activating immune cells using the model RAW-Blue cells, a RAW 264.7 macrophage cell line with chromosomal integration of a secreted embryonic alkaline phosphatase (SEAP) reporter. The overall SEAP levels in the culture media, reflecting IS activity, was determined by a colorimetric enzyme assay using the QUANTI-Blue agent (Scheme S1 in Supporting information). As shown in Fig. 2c, the IS activity of CA and CHA increased by 1.7-fold and 2-fold with the incubation time increased from 2 h to 16 h respectively, while HA nearly had no IS activity.

To investigate the efficacy of NIR-II light induced cancer cell death, a key step *in-situ* generating TAAs for immune activations, we determined the cytotoxicity of either single NA or cocktail NA formulations in presence or absence of 1064-nm light irradiations. In absence of NIR-II light irradiation, all NA formulations did not show toxicity to 4T1 cells throughout the whole texted concentrations (Fig. 2d). In contrast, in the presence of NIR-II light irradiation, all AuNS-containing NAs (HA, CHA and the cocktail NAs with different CA to HA ratios) showed a concentration-dependent cytotoxicity (Fig. 2e), while CA groups did not show any toxicity even when their concentration reached as high as 40 μg/mL because of their incapability in adsorbing NIR-II light.

To compare the *in vivo* efficacy of immune-responses among various treatments, particularly the comparison between integrated NA formulation (CHA) and cocktail NAs (cNAs), we examined the maturated dendritic cells (mDCs) in tumor-draining lymph nodes (TDLNs) and T-cells proliferation both in tumors and spleens, following the flowchart as shown in Fig. 3a. Firstly, the expression levels of mDCs within TDLNs were determined by the flow cytometry analysis after triple-staining of DCs with CD11c-FITC (fluorescein isothiocyanate labeled CD11c monoclonal antibody), CD80-APC (antigen-presenting cells CD80 antibody) and CD86-PE (R-phycoerythrin-labeled CD80 antibody) (the detail experimental procedures were shown in Supporting information). Comparing with the control saline treatment, upon irradiation with 1064 nm light, CA and HA only induced a slight increase on the mDC expression, while CHA showed 1.6-fold enhancement of mDC (Fig. 3b). Interestingly, cocktail NAs, bearing 1 equiv. of CpG and AuNS with CHA, showed an even higher mDC levels within TDLNs than CHA.

Along with mDCs, T-cells are also essential in eliciting effective immune responses against cancer cells. In particular, $CD4^+$ helper T cells and $CD8^+$ killer T cells are important sub-family effector cells in mediating the vaccine-based immunotherapy, where the former plays a major role in instigating and shaping adaptive immune responses, while the latter is responsible for elimination of cancer cells and can provide long-term protective immunity [25,26]. Therefore, we analyzed the infiltration of $CD4^+$ and $CD8^+$ T cells in tumors upon treatments with CA, HA, CHA and cNAs plus NIR-II light irradiation. As shown in Fig. 3c, comparing with saline group, all NA formulations showed a significant enhancement on the expression of $CD4^+$ and $CD8^+$ T cells, while with different degrees, following the order of CA ≈ HA < CHA < cNA. Similarly,

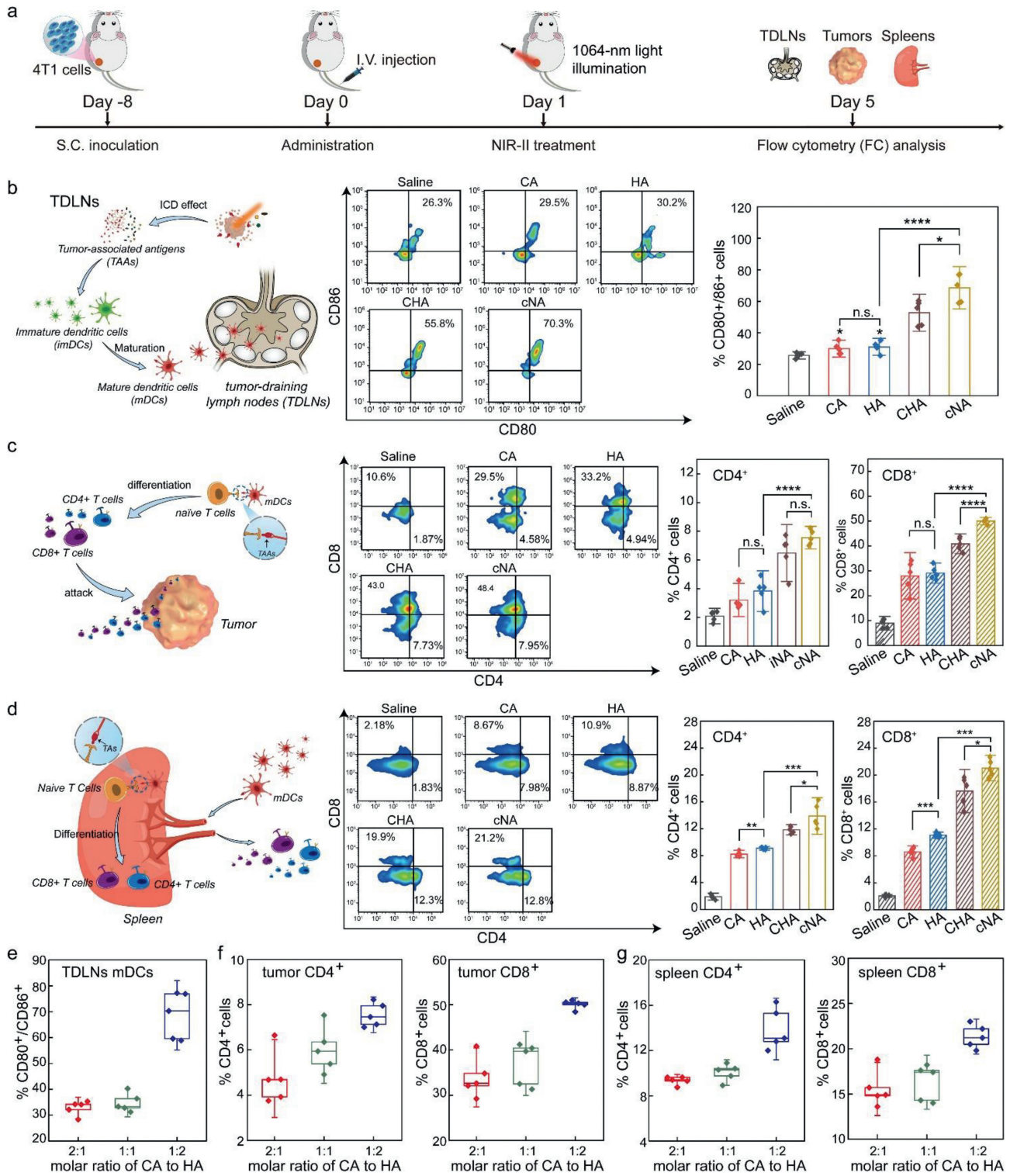

Fig. 3. *In vivo* immune response analysis of NIR-II light induced DCs mutation and T cells differentiation with different formulations of NAs. (a) The timeline of *in vivo* evaluations. (b-d) Flow cytometry analysis of DCs mutation within TDLNs (b), proliferation of T-cells within tumors (c) or spleens (d). (e-g) Molar ratio effect of CA:HA on the immunostimulation. Data were expressed as means ± S.E.M. ($n = 3$) with the significant differences (P values) determined by the unpaired double-tailed t test, $^{*}P < 0.05$, $^{**}P < 0.01$, $^{***}P < 0.005$, $^{****}P < 0.001$ and n.s. means no significant difference.

elevated levels of $CD4^+$ and $CD8^+$ T cells within spleens were also observed by NA treatments (Fig. 3d), and the cocktail formulation showed the highest T cell proliferations.

Next, to investigate how the ratio of two components (CA and HA) in cNA influences the NIR-II-triggered immune responses, we determined the mDCs within TDLNs and T cells in tumors and spleens (including $CD4^+$ and $CD8^+$ T cells) upon treatments with three CA/HA ratios (2:1, 1:1 and 1:2). Interestingly, with the increase of HA component, both mDCs and T cells increased correspondingly, particularly for the 1:2 formulation, where a dramatic enhancement of immune cells were clearly observed comparing with the other two formulations (Figs. 3e–g). These results

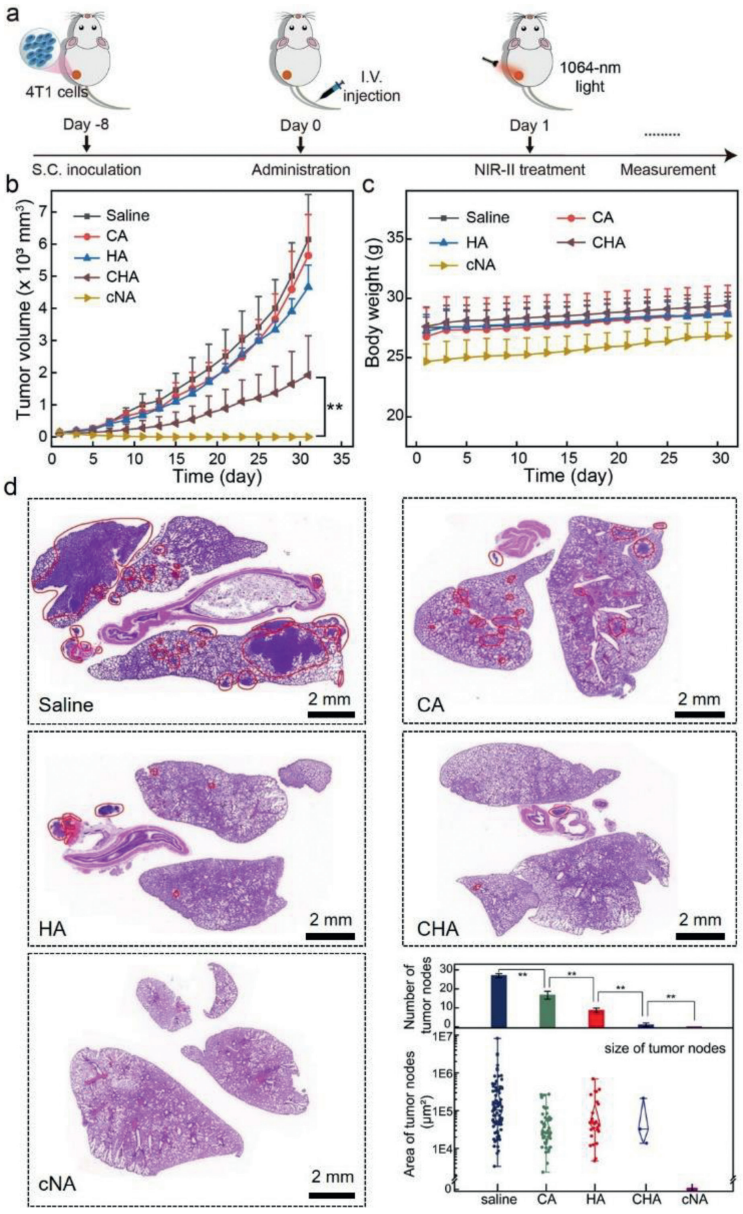

Fig. 4. Cocktail NAs showed an enhanced tumor-inhibition effect and completely inhibited the pulmonary metastases. (a) Timeline of anticancer evaluations. (b) Tumor-growth curve as a function of time after different treatments. Data are expressed as means ± S.E.M. ($n = 6$), $^{**}P < 0.01$. (c) Mice body weight as a function of time post-treatment with different NA formulations. (d) Full-scale images of H&E-stained lung slices from mice 30 days after the NIR-II irradiation at the tumor site for saline, CA, HA, CHA or cNA administrated mice respectively. Data at the bottom-right corner represent the average number of tumor nodules counted from the H&E-stained lung slices and the size of tumor nodules measured *via* ImageJ software for different treatment Groups. Data are expressed as means ± S.E.M. ($n = 3$) with the significant differences determined by the unpaired double-tailed t test, $^{**}P < 0.01$.

indicated that within the cocktail formulation, HA had a higher influence on the NIR-II-triggered immune responses than CA did.

Based on the promising anticancer immune responses of cNAs, we examined whether cNAs could bring enhanced effect of tumor-growth inhibition upon the NIR-II light irradiation. One day post-i.v.-injection with 4 formulations of NAs (CA, HA, CHA, or cNA), local irradiation on the tumor site with a 1064 nm light for 5 min was performed and then tumor volumes in each group were measure every other day (Fig. 4a). Results showed that the tumors from saline, CA and HA groups were growing rapidly over time. Particularly after 13 days, the tumor growth from these groups displayed an exponential growth character (Fig. 4b). In contrast, the tumors in CHA group grew relatively slowly in 25 days post irradiation, and it is worthwhile noting that there was one mouse whose tumor disappeared on Day 21 with no recurrence over the entire observation time. Interestingly, in cNA group, the tumors from all six mice did not grow but shrink over time: there were 2 mice whose tumor disappeared on Day 17, while the tumors in other 4 mice disappeared on Day 21, and what's more, no cancer recurrence in these 6 mice was overserved over the entire observation time. Body weight analysis indicated that the two components of cNA had good biocompatibility (Fig. 4c) and did not induce significant toxicity against the normal organs as shown in our previous publication [19]. The above results indicated that both the photothermal agent AuNS and immunostimulatory CpG are indispensable ingredients in eliciting effective anticancer immunotherapy. Moreover, the cocktail formulation of NAs is much more suitable in pursuit of the optimal ISTV efficacy than the "all-in-one" integrated formulation (Fig. S3 in Supporting information).

Subsequently, we evaluated whether the excellent tumor-growth inhibition effect by cNA could also lead to a better inhibitory effect of pulmonary metastases, a commonly occurred

secondary malignant tumors of the lung parenchyma or pleura originating from the other site of the body, which is also an important index to evaluate the efficacy of vaccines-based immunotherapies. At the end of the above tumor-growth inhibition experiment, the lungs from each group were collected, sliced and stained with hematoxylin and eosin (H&E) for possible tumor nodules observations. Comparing with saline group, where a large number of tumor nodules with the average sizes ranging from 3×10^3 μm^2 to 8×10^6 μm^2 was observed in H&E-stained lung slices (Fig. 4d), tumor nodules from CA, HA and CHA groups were much less and smaller, following the order of CHA < HA < CA. Interestingly, no tumor nodules could be found in the lung slices from cNA group. These results indicated that cNAs, instead of CHA, combined with NIR-II light irradiation could successfully prevent tumor invasion and metastases to the lung. Moreover, the inhibitory efficacy of cNAs + NIR-II against pulmonary metastases increased with the molar ratio of HA to CA (Fig. S4 in Supporting information).

Finally, we determined the hemocompatibility of each NP formulation *via* the hemolysis test. Results showed that no hemolysis occurred for either CA or HA even when their concentrations reached as high as 50 μg/mL (Fig. S5 in Supporting information), providing an essential prerequisite for their *in vivo* applications.

In conclusion, a "cocktail" nano-adjuvant formulation was prepared by physically mixing the photothermal constitute HA and the immunostimulatory constitute CA. CpG-containing nano-adjuvant exhibited a much higher cell uptake efficacy than only-HAase-containing sample for both tumor cells and immune cells. Compared to "all-in-one" formulation, the "cocktail" nano-adjuvants displayed a much higher NIR-II-triggered ISTV effects, including DCs mutation in tumor-draining lymph nodes and T-cells proliferation both in tumors and spleens. What is more, increasing the molar ratio of HA to CA led to an enhanced anticancer immune responses. Finally, "cocktail" nano-adjuvant showed higher inhibition effects on tumor-growth and pulmonary metastases.

Declaration of competing interest

The authors declare that they have no known competing financial interests or personal relationships that could have appeared to influence the work reported in this paper.

Acknowledgments

This work was financially supported by the National Natural Science Foundation of China (No. 52273163), the Science Technology and Innovation Commission of Shenzhen Municipality (No. JCYJ20190807163003704), and Open Research Fund of Jiangsu Key Laboratory of Environmentally Friendly Polymeric Materials (No. PML2201).

Supplementary materials

Supplementary material associated with this article can be found, in the online version, at doi:10.1016/j.cclet.2023.108443.

References

[1] Z.M. Li, W.G. Xu, J.Z. Yang, et al., Adv. Mater. 34 (2022) 2200449.
[2] Q. Wei, L.N. Zhang, N. Zhao, et al., Front. Immunol. 13 (2022) 1012927.
[3] W.G. Xu, Y.Z. Su, Y. Ma, et al., Sci. China Chem. 66 (2023) 1150–1160.
[4] J. Zhang, Y.D. Lin, Z. Lin, et al., Adv. Sci. 9 (2022) 2103444.
[5] P. Zheng, B.B. Ding, Z.Y. Jiang, et al., Nano Lett. 21 (2021) 2088–2093.
[6] Y.Z. Su, W.G. Xu, Q. Wei, et al., Sci. Bull. 68 (2023) 284–294.
[7] X.R. You, L.Y. Wang, L. Wang, J. Wu, Adv. Funct. Mater. 31 (2021) 2100805.
[8] H.X. Zhang, X.R. You, X.J. Wang, et al., Proc. Natl. Acad. Sci. U. S. A. 118 (2021) e2005191118.
[9] X.R. You, L.Y. Wang, J.F. Zhang, et al., Chin. Chem. Lett. 34 (2023) 107720.
[10] Z.W. Fang, X.Y. Zhang, H. Huang, J. Wu, Chin. Chem. Lett. 33 (2022) 1693–1704.
[11] R.X. Chen, P. Ouyang, L.C. Su, et al., Chin. Chem. Lett. 33 (2022) 4610–4616.
[12] J.J. Chen, M. Qiu, Z.F. Ye, et al., Sci. Adv. 7 (2021) eabf1244.
[13] Y.Y. Hu, L. Lin, Z.P. Guo, et al., Chin. Chem. Lett. 32 (2021) 1770–1774.
[14] X. Li, Y.X. Zhang, X.H. Wu, et al., Small 18 (2022) 2203100.
[15] M.J. Lin, J. Svensson-Arvelund, G.S. Lubitz, et al., Nat. Cancer 3 (2022) 911–926.
[16] X.Y. Shen, C.J. Zhu, X.T. Liu, et al., Biomater. Sci. 11 (2023) 1137–1152.
[17] X.F. Zhong, X. Sun, Acta Pharmacol. Sin. 41 (2020) 928–935.
[18] Z.S. Morris, E.I. Guy, D.M. Francis, et al., Cancer Res. 76 (2016) 3929–3941.
[19] A.H. Chen, L. Wu, Y. Luo, et al., Small 18 (2022) 2200993.
[20] Q. Liu, J.W. Tian, Y. Tian, et al., ACS Nano 15 (2021) 515–525.
[21] Y.C. Ma, Y.X. Zhang, X.Q. Li, et al., ACS Nano 13 (2019) 11967–11980.
[22] Y.F. Zhang, T.J. Song, T. Feng, et al., Nano Today 35 (2020) 100987.
[23] J. Yue, R.M. Pallares, L.E. Cole, et al., ACS Appl. Mater. Inter. 10 (2018) 21920–21926.
[24] C.H.J. Choi, L.L. Hao, S.P. Narayan, E. Auyeung, C.A. Mirkin, Proc. Natl. Acad. Sci. U. S. A. 110 (2013) 7625–7630.
[25] S. Hadrup, M. Donia, P.T. Straten, Cancer Microenviron. 6 (2013) 123–133.
[26] M. Reina-Campos, N.E. Scharping, A.W. Goldrath, Nat. Rev. Immunol. 21 (2021) 718–738.